Effective reaction rates in diffusion-limited phosphorylation-dephosphorylation cycles

Paulina Szymańska*
College of Inter-Faculty Individual Studies in Mathematics and Natural Sciences, University of Warsaw, 02-089 Warsaw, Poland

Marek Kochańczyk*
Institute of Fundamental Technological Research, Polish Academy of Sciences, 02-106 Warsaw, Poland

Jacek Miękisz
Institute of Applied Mathematics and Mechanics, University of Warsaw, 02-097 Warsaw, Poland

Tomasz Lipniacki†
Institute of Fundamental Technological Research, Polish Academy of Sciences, 02-106 Warsaw, Poland and Department of Statistics, Rice University, Houston, Texas 77005, USA

(Received 10 April 2014; revised manuscript received 10 June 2014; published 3 February 2015)

We investigate the kinetics of the ubiquitous phosphorylation-dephosphorylation cycle on biological membranes by means of kinetic Monte Carlo simulations on the triangular lattice. We establish the dependence of effective macroscopic reaction rate coefficients as well as the steady-state phosphorylated substrate fraction on the diffusion coefficient and concentrations of opposing enzymes: kinases and phosphatases. In the limits of zero and infinite diffusion, the numerical results agree with analytical predictions; these two limits give the lower and the upper bound for the macroscopic rate coefficients, respectively. In the zero-diffusion limit, which is important in the analysis of dense systems, phosphorylation and dephosphorylation reactions can convert only these substrates which remain in contact with opposing enzymes. In the most studied regime of nonzero but small diffusion, a contribution linearly proportional to the diffusion coefficient appears in the reaction rate. In this regime, the presence of opposing enzymes creates inhomogeneities in the (de)phosphorylated substrate distributions: The spatial correlation function shows that enzymes are surrounded by clouds of converted substrates. This effect becomes important at low enzyme concentrations, substantially lowering effective reaction rates. Effective reaction rates decrease with decreasing diffusion and this dependence is more pronounced for the less-abundant enzyme. Consequently, the steady-state fraction of phosphorylated substrates can increase or decrease with diffusion, depending on relative concentrations of both enzymes. Additionally, steady states are controlled by molecular crowders which, mostly by lowering the effective diffusion of reactants, favor the more abundant enzyme.

DOI: 10.1103/PhysRevE.91.022702 PACS number(s): 87.10.Hk, 82.20.Pm, 87.10.Rt, 87.15.A−

I. INTRODUCTION

Cellular information is transmitted and processed by complex networks of coupled biochemical reactions. Dynamics of these networks is governed by reaction rates, which are strongly influenced by diffusivity of reactants [1], their subcellular localization, and nonspecific molecular crowding [2–4].

The aim of our study is to analyze the dependence of effective macroscopic reaction rate coefficients on diffusion in cycles of coupled antagonistic reactions. Such cycles, exemplified by the phosphorylation-dephosphorylation cycle or the GTPase cycle (Fig. 1), are crucial for cellular signal transduction. In the ubiquitous motif of the phosphorylation-dephosphorylation cycle, substrate molecules are phosphorylated and dephosphorylated by kinases and phosphatases, respectively. For example, in the GTPase cycle [5], GTPases such as Ras exist in either of two signaling states: GTP-bound Ras is active (as it can recruit Raf and trigger MAPK kinase cascade signaling), while GDP-bound Ras is inactive. GTPase-activating proteins (GAPs) assist in the transition from the GTP-bound to GDP-bound forms, while guanine nucleotide-exchange factors (GEFs) facilitate GDP dissociation followed by reloading of Ras with GTP. Overall, reversible regulatory motifs allow for substrate reuse and signal amplification, thus enabling rapid transmission of extracellular signals to effector proteins such as transcription factors.

In this study we focus on chemical kinetics in two-dimensional systems such as biological membranes. The two-dimensional (2D) systems have their own peculiarities and significantly differ from 3D systems but are very important for signal transduction. Signal transduction in numerous pathways is initiated by cytokine binding to membrane receptors, which transmit signal to secondary messengers, often by phosphorylation. Plasma membrane is a very crowded and nonhomogenous environment where reactions are expected to be diffusion controlled. This distinguishes plasma membrane from the cytoplasm, which is characterized by at least one order of magnitude faster diffusion and in which the characteristic reaction time scale is longer.

Since the seminal work of von Smoluchowski on kinetics of diffusion-limited association [6], there have been numerous attempts to derive effective macroscopic reaction rate coefficients (EMRRCs) that govern processes in a macroscale chemical reactor. These derivations were based mostly on

*These authors contributed equally.
†tlipnia@ippt.pan.pl

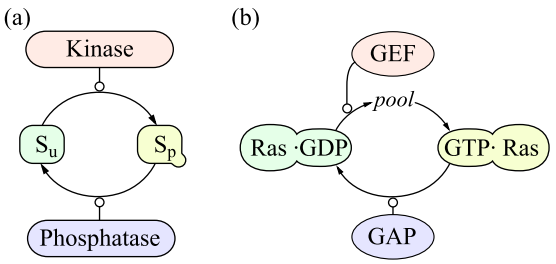

FIG. 1. (Color online) (a) A simple phosphorylation-dephosphorylation cycle; S_u, dephosphorylated substrate; S_p, phosphorylated substrate. (b) Ras GTPase cycle; GEF, guanine nucleotide-exchange factor; GAP, GTP-ase activating protein.

microscopic models having a single-molecule resolution, continuous in space and time. Halfway between, the system can be described by means of a reaction-diffusion master equation, referred to as mesoscopic, as it averages out the kinetics over the microscopic length and time scales [7,8]. We will approach the microscopic limit by means of on-lattice kinetic Monte Carlo simulations, assuming that each lattice site can be either occupied by one molecule or empty. This approach, in contrast to mesoscopic description-based simulation methods, provides us with the single-molecule and single-reaction resolution, but simplifies the continuous space to a discretized lattice.

Reaction schemes studied thus far can be divided into reversible and irreversible. For the reversible case, even in equilibrium, reactions still take place and the steady state may be nontrivial. For the irreversible case, the system converges in most cases to a well-defined state in which all reactions cease; but the determination of time-dependent behavior still remains a challenging problem.

Irreversible reaction systems are as follows:

$A + B \to C$: Collins and Kimball [1] determined the time-dependent reaction rate in the case when only a fraction of collisions leads to dimer formation (extending the study of von Somoluchowski [6]) and analyzed two limits corresponding to diffusion control and reaction (activation energy) control. Further works by Naqvi [9], Emais and Fehder [10], and Torney and McConnel [11] showed essential differences between two- and three-dimensional systems. In three dimensions, the reaction rate "quickly" stabilizes at some positive value, while in two dimensions it decreases to zero as $1/\ln(t)$ [11]. A very similar reaction, $A + B \to \emptyset$, was considered by Toussaint and Wilczek in the context of particle-antiparticle annihilation [12] (see also Ref. [13]).

$A + B \to A + C$ and $A + B \to AB \to A + C$: Szabo considered this unidirectional reaction in the context of fluorescent quenching, where A is a quencher and B (C) are in excited (relaxed) states [14]. By employing various approaches, including that of von Smoluchowski, mean-field, mean first-passage time, he calculated the reaction rate to find that the agreement between these approaches is satisfactory only in the limit of small concentration and fast diffusion. For the Michaelis-Menten scheme, $A + B \rightleftharpoons AB \to A + C$, Kim *et al.* found that the long-time asymptotic relaxation of the deviation of the bound enzyme concentration from the steady-state value shows the power-law behavior $\propto (Dt)^{-1/2}$, where D is the diffusion coefficient [15]. The same scheme has been analyzed by Park and Agmon [16,17]. In the latter work, Park and Agmon determined substrate concentration profiles developing near a static enzyme molecule. Also Zhou developed theoretical approaches and performed simulations to quantify the diffusion influence on binding and unbinding rates [18].

Reversible reaction systems are as follows:

$A + B \rightleftharpoons C$: Classical mass-action theory in the limit of infinite diffusion predicts exponential relaxation to the steady state. For diffusion-influenced kinetics, Zel'dovich and Ovchinnikov showed that the system follows power-law relaxation $\propto (Dt)^{-3/2}$ in 3D [19]. Then Berg calculated the diffusion-controlled dissociation constant [20], and, later, Agmon and Szabo determined the time-dependent kinetics for the fraction of dissociated A and B molecules for various initial and boundary conditions [21,22]. Szabo discussed three different approaches to the relaxation kinetics of the reversible association reactions that lead to nonexponential relaxation in the diffusion-limited case [22]. Sung and Lee provided an accurate theory of the diffusion-influenced reversible association reactions [23] which is in agreement with numerical results of Edelstein and Agmon [24] and correctly reduces to the von Smoluchowski's result in the irreversible limit. Takahashi *et al.* [25] considered a more complex double phosphorylation-dephosphorylation cycle based on this simple reaction scheme. They found that substrate rebindings, which arise more likely for slow diffusion, turn a distributive phosphorylation mechanism into a processive one leading to the loss of ultrasensitivity in the MAPK cascade. Processive phosphorylation is the mechanism of double phosphorylation happening at a single enzyme-substrate encounter. This phosphorylation mode is favored in the case of slow diffusion. In the distributive phosphorylation mechanism, occurring more likely for faster diffusions, the subsequent phosphorylations happen at different enzyme-substrate collisions and may be performed by different enzyme molecules. Recently, substrate rebinding was considered by van Zon *et al.*, who found that repressor-promoter rebindings slow down gene switching and therefore increase gene expression noise [26]. In the context of T-cell receptor (TCR) activation it was found that fast TCR-pMHC rebindings of shortly bound ligands can allow for kinetic proofreading-based TCR activation similar to that induced by ligands which bind for longer times [27].

$A + B \rightleftharpoons C + D$: In a series of papers, Agmon and colleagues obtained analytical solutions for the Green function and survival probabilities of the reversible reaction. They found that the asymptotic state (in three dimensions) is reached as $(Dt)^{-1/2}$, as in the irreversible case [28–30]. Recently, for the reversible Michaelis-Menten scheme, $A + B \rightleftharpoons AB \rightleftharpoons A + C$, Szabo and Zhou calculated the steady-state reaction rates in the case when substrate and product concentrations are effectively fixed, so bimolecular reactions can be treated as pseudo first order [31]. They found that, similarly to the irreversible Michaelis-Menten kinetics, the relaxation of free- and bound-enzyme concentrations to steady state follows the power law $\propto (Dt)^{-1/2}$.

The molecular crowding effect was studied and discussed in a considerable number of papers and reviews [2–4]. To-date results state that crowding, acting through volume exclusion, influences the reactions rates differently in different regimes.

In the diffusion-controlled regime it decreases the effective rate coefficients, whereas it increases them in the reaction-controlled regime. Also, it creates microdomains that can transiently cage substrates or enzymes [3,32–34]. In particular, it was shown experimentally and analyzed theoretically that substrate caging can change the distributive phosphorylation mode into the processive one [35]. Recently, it was shown by Weiss that molecular crowding renders fluids viscoelastic, which in turn leads to subdiffusion of tracer particles [36].

In this work we investigate the phosphorylation-dephosphorylation cycle consisting of two opposing reactions: $K + S_u \to K + S_p$ and $P + S_p \to P + S_u$, and analyze how EMRRCs and steady states depend on the diffusion and concentrations of enzymes (kinases, K, and phosphatases, P). In the considered model, the nonuniformity in spatial distribution of phosphorylated and dephosphorylated substrates is inherent to the system. At small densities of enzymes, each enzyme molecule is surrounded by a cloud of converted substrates. Since the scale of nonuniformity is controlled simultaneously by both enzymes, the effective phosphorylation and dephosphorylation rate coefficients are expected to be coupled.

The paper is organized as follows: In Sec. II we define our models and outline the methods used for numerical analysis; in Sec. III we provide analytical solutions for limiting cases; and in Sec. IV we present numerical results and highlight interesting effects. Discussion follows in Sec. V.

The paper is supplemented with four appendices: In Appendix A we show that EMRRCs are independent of the lattice size for sufficiently large lattices; in Appendix B we analyze the dependence of macroscopic diffusion on motility and density of molecules; in Appendix C we analyze nonequilibrium dynamics of the system of two opposing reactions (i.e., the basic model) and the system without the dephosphorylation reaction; and in Appendix D we consider a model variant in which phosphorylation and dephosphorylation proceed via formation of a transient enzyme-substrate complex.

II. MODELS AND METHODS

A. Numerical methods

All of the considered models introduced hereafter are analyzed by means of spatial kinetic Monte Carlo (KMC) simulations [37,38]. Molecules are placed on discrete sites of a two-dimensional triangular lattice which forms a square domain with periodic boundary conditions. The molecules diffuse freely by hopping to adjacent empty lattice sites. Their state can be modified due to chemical reactions, either unimolecular or bimolecular (involving two molecules occupying adjacent lattice sites). Diffusion and reaction events occur at defined rates called motilities and (microscopic) reaction rate constants, respectively. Motilities, m, are assumed to be equal for molecules of all types (unless otherwise specified). The propensity of hopping to a neighboring empty site on the triangular lattice is $m/6$. All allowed chemical reactions are defined together with their respective reaction rate constants.

At each step of the KMC simulation, a list of all events possible on the lattice is available. Time step is drawn at random from the exponential distribution with the rate parameter equal to the sum of the rates of all possible events. A diffusion or reaction event is selected from the complete events list at random, with probability proportional to its rate. This approach is equivalent to a stochastic simulation according to the Gillespie algorithm [39] extended to account for additional diffusive events. Such construction allows for direct comparison of motility with reaction rate constants. After every event, the list of all events is updated. However, since the change in the system configuration after every simulation step is local, only a partial update of the list is necessary. By drawing events from the always-complete list, there is no need to simulate trial events that would be subsequently rejected, rendering the method efficient. The overall algorithm is essentially equivalent to the Bortz-Kalos-Lebowitz method applied previously to, e.g., studying dynamics of Ising spin glasses [40].

Initial distribution of molecules on the lattice is uniformly random. Simulations were performed on the 100×100 lattice to estimate EMRRCs in equilibrium; in the nonequilibrium case, the 300×300 lattice was used in order to obtain better statistics, while the spatial correlation functions were determined based on simulations performed on the 500×500 lattice. As shown in Appendix A, simulations performed on lattices of sizes equal or larger than 30×30 with a number of molecules of each type exceeding 50, give the EMRRCs estimates independent of the lattice size. EMRRCs in equilibrium were determined by averaging over 10 independent, long-run simulations of the system in equilibrium (assessed by invariance of nontrivial radial distribution functions or correlation length-based considerations [41]). Unless stated otherwise, the simulations were preceded by equilibration phase of 1000 and lasted at least 1000 each. In the nonequilibrium case we performed 1000 independent simulations to obtain satisfactory statistics (see Appendix C for further details).

Numerical results are supplemented by analytical expressions obtained in two extreme cases of zero and infinite motility. We also analyze how the steady states and effective motilities are influenced by nonspecific molecular crowders of varying motilities.

B. Phosphorylation-dephosphorylation cycle

We consider a phosphorylation-dephosphorylation cycle assuming that these processes are unidirectional reactions, occurring at their respective rates; the free energy expenditure featuring reaction cycles is neglected. Substrates are phosphorylated and dephosphorylated by kinases and phosphatases according to the following set of reactions:

$$K + S_u \xrightarrow{c} K + S_p, \tag{1a}$$

$$P + S_p \xrightarrow{d} P + S_u, \tag{1b}$$

where S_u and S_p stand for dephosphorylated and phosphorylated substrates, respectively, and K represents the kinase and P the phosphatase. The symbols ρ_K, ρ_P, ρ_{S_u}, and ρ_{S_p} will denote surface densities, i.e., the fractions of lattice sites occupied by respective molecules. Coefficients c and d are the microscopic rate constants of phosphorylation and dephosphorylation reactions catalyzed by adjacent enzymes. In other words, c and d are propensities of respective reactions when an enzyme molecule is in contact with a substrate molecule.

Equations (1) should not be read as exact chemical balance equations; instead, they conform to an approximation in which the concentration and diffusion coefficient of ATP (phosphate donor) are sufficient to assume that ATP accessibility does not limit the phosphorylation reaction rate. Also the inorganic phosphate molecules produced in dephosphorylation reactions are not taken into account.

As a reference to the basic model defined by Eqs. (1) we also consider a model variant in which dephosphorylation is a first-order reaction, i.e.,

$$S_p \xrightarrow{d_0} S_u, \tag{2}$$

whereas phosphorylation still occurs via Eq. (1a). The *first-order dephosphorylation* (FOD) reaction is a simplification but it serves as an approximation when a particular phosphatase or its level are unknown. In order to compare FOD approximation with the basic model, we set $d_0 = 6\rho_P d$, which assures equal dephosphorylation efficiencies in the limit of infinite motility, as will be shown later.

The basic model does not account explicitly for the formation of the enzymatic encounter complex: Both the phosphorylation and dephosphorylation are considered to be single-step reactions. In reality, these reactions are multistep processes (enzyme-substrate binding, catalytic reaction, and enzyme-product dissociation). As shown in the Appendix D, this simplification does not significantly affect our key findings, at least when the enzyme sequestration is weak.

C. Macroscopic description and effective reaction rate coefficients

Time evolution of systems of reacting molecules is usually described by chemical mass-action kinetics equations, i.e., systems of ordinary differential equations for densities of substrates and products. Here we take into account the spatial and discrete nature of biochemical reactions and simulate numerically processes involving individual molecules. Our aim is to determine—based on the microscopic rate constants c and d—the effective reaction rate coefficients, which can be then used in the macroscopic description of the system.

We define the *effective macroscopic phosphorylation rate coefficient* c_{eff} and *effective macroscopic dephosphorylation rate coefficient* d_{eff} accordingly:

$$c_{\text{eff}} = \frac{n}{\rho_{S_u}\rho_K V \Delta t}, \tag{3a}$$

$$d_{\text{eff}} = \frac{n}{\rho_{S_p}\rho_P V \Delta t}, \tag{3b}$$

and refer to them collectively as to EMRRCs. In Eqs. (3), n is the number of (de)phosphorylation reactions that fired during a time interval Δt and V is the lattice surface area (i.e., total number of lattice sites). The densities of kinases, phosphatases, and substrates are denoted by ρ with a respective subscript: ρ_K, ρ_P, ρ_{S_u}, and ρ_{S_p}.

For the most part in our study, we will focus on the steady-state analysis where EMRRCs can be estimated based on long-run simulations, in which the number of reactions is determined over a satisfactorily long time interval Δt. Only in Appendix C will we perform simulations for the system which is initially far from equilibrium to show that for the reversible phosphorylation-dephosphorylation cycle EMRRCs converge to their steady states. In this case, we will estimate EMRRCs within short time intervals by averaging over 1000 independent KMC simulations.

When the number of molecules present in the system is large we can write the following system of ordinary differential equations:

$$\frac{d}{dt}\rho_{S_u} = -c_{\text{eff}}\rho_K\rho_{S_u} + d_{\text{eff}}\rho_P\rho_{S_p}, \tag{4a}$$

$$\frac{d}{dt}\rho_{S_p} = c_{\text{eff}}\rho_K\rho_{S_u} - d_{\text{eff}}\rho_P\rho_{S_p}. \tag{4b}$$

These two equations are complementary, since their solutions satisfy $\rho_{S_u}(t) + \rho_{S_p}(t) = \rho_S = \text{const}$. The steady-state solution of Eqs. (4) reads:

$$\rho_{S_u} = \frac{d_{\text{eff}}\rho_P}{c_{\text{eff}}\rho_K + d_{\text{eff}}\rho_P}\rho_S, \tag{5a}$$

$$\rho_{S_p} = \frac{c_{\text{eff}}\rho_K}{c_{\text{eff}}\rho_K + d_{\text{eff}}\rho_P}\rho_S. \tag{5b}$$

In the next section we will analyze the dependence of the steady-state solutions and EMRRCs on motility. EMRRCs provide more information than steady states alone; for example, they give the ATP turnover which can be measured by radioactively labeled ATP (γ-^{32}P-ATP). First, we will provide analytical results in the limits of zero and infinite motility. Then we will analyze numerically our model for finite, nonzero motilities.

III. ANALYTICAL RESULTS

A. Infinite-motility limit

We assume that in the *infinite-motility limit* the probability of finding a given molecule is uniform on the lattice. Thus, at any time the density of enzyme-substrate pairs is given by the product of densities multiplied by the number of potential neighbors, e.g., the kinase-dephosphorylated substrate pair density is equal to $6\rho_K\rho_{S_u}$. Therefore, the phosphorylation rate, i.e., the number of phosphorylation reactions per reactor volume per time, is equal to $6c\rho_K\rho_{S_u}$, which in light of Eq. (4) gives $c_{\text{eff}}^{\infty} = 6c$. The limit of infinite motility will be compared later with simulations performed for high motilities.

B. Zero-motility limit

The *zero-motility limit* is a singular limit, since without mixing the whole process is determined by initial positions of enzymes and substrates. For an arbitrarily small motility, however, the system relaxes after a sufficiently long time.

The zero-motility limit approximates the behavior of dense systems, in which diffusion is substantially reduced, but reactions still occur for substrates in the close vicinity of opposing enzymes. Increased density, together with reduced diffusion, features receptor clusterization, necessary, for example, for the initiation of B-cell receptor signaling [42–45] and TLR4-CD14 cluster formation preceding receptor internalization [46]. Formation of dense ordered patterns of proteins and other molecules has been intensively modeled in recent years (see Ref. [47] and references therein).

We start the analysis of this limit by calculating the steady-state densities of phosphorylated and dephosphorylated substrates, ρ_{S_p} and ρ_{S_u}:

$$\rho_{S_p} = p^+ \cdot \rho_S, \quad \rho_{S_u} = \rho_S - \rho_{S_p}, \tag{6}$$

where p^+ is the probability that a substrate molecule is in the phosphorylated state.

When the motility is zero, the probability that a given substrate molecule is phosphorylated depends solely on the number of neighboring kinases, i, and the number of neighboring phosphatases, j, and is equal to

$$p^+_{ij} = \frac{ic}{ic + jd}. \tag{7}$$

The probability of having exactly i kinase and j phosphatase neighbors is

$$p_{ij} = \binom{6}{i} \rho_K^i \binom{6-i}{j} \rho_P^j (1 - \rho_K - \rho_P)^{6-i-j}, \quad i,j \in \{0,1,\ldots,6\}, \quad 1 \leqslant i + j \leqslant 6 \tag{8}$$

and the probability that the substrate is in the phosphorylated state without contact with any enzyme molecule is equal to the probability that the substrate is in the phosphorylated state while in contact with at least one enzyme molecule. The Eq. (8) is exact only on infinite domains with infinite number of kinases and phosphatases; however, it serves as a good approximation when the number of enzymes of each type is much larger than 1. The infinitely small but nonzero motility means that substrates equilibrated in contact with the enzyme diffuse away maintaining their phosphorylation status which cannot change without a subsequent contact with an appropriate enzyme molecule.

Therefore, the probability p^+ is given by the conditional probability that a substrate molecule is phosphorylated when in contact with at least one enzyme molecule,

$$p^+ = \sum_{1 \leqslant i+j \leqslant 6} p_{ij} p^+_{ij} \Big/ \sum_{1 \leqslant i+j \leqslant 6} p_{ij}, \tag{9}$$

where the sum runs over all substrate molecules having contact with at least one enzyme molecule.

Now we will calculate EMRRCs in the steady state. Let us notice that in the zero-motility limit reactions occur only for the substrate molecules which have neighbors of different types (i.e., at least one kinase and one phosphatase). Let us recall that the probability that the substrate which has i neighboring kinases and j neighboring phosphatases is dephosphorylated is $jd/(ic + jd)$. The phosphorylation propensity is ic for the unphosphorylated substrate, while it is 0 for the phosphorylated substrate. Thus the effective phosphorylation propensity is $ic\,jd/(ic + jd)$. In the stationary state the number of the phosphorylation and dephosphorylation reactions per reactor volume per time must be equal, and thus the reaction rates are equal to $\rho_S \sum_{i,j \geqslant 1, i+j \leqslant 6} p_{ij}(ic\,jd)/(ic + jd)$ and, correspondingly, the effective phosphorylation and dephosphorylation rate coefficients are equal to

$$c^0_{\text{eff}} = \frac{\rho_S}{\rho_K \rho_{S_u}} \sum_{\substack{i,j \geqslant 1 \\ i+j \leqslant 6}} p_{ij} \frac{ic\,jd}{ic + jd}, \tag{10a}$$

$$d^0_{\text{eff}} = \frac{\rho_S}{\rho_P \rho_{S_p}} \sum_{\substack{i,j \geqslant 1 \\ i+j \leqslant 6}} p_{ij} \frac{ic\,jd}{ic + jd}, \tag{10b}$$

where $\rho_S/\rho_{S_u} = 1/(1 - p^+)$ and $\rho_S/\rho_{S_p} = 1/p^+$, with p^+ given by Eq. (9).

One should keep in mind that rate coefficients c^0_{eff} and d^0_{eff} were derived under the steady-state assumption and, therefore, far from equilibrium their values can be substantially different. The phosphorylation and dephosphorylation rate coefficients obtained in the limit of zero motility give the lower bounds for EMRRCs. In the limit of $\rho_K \to 0$ and $\rho_P \to 0$, Eq. (8) implies $p_{ij} \approx p_{11} = 30\rho_K\rho_P$ (the probability of having more than one enzyme of each kind is negligibly small, so $p_{ij} = 0$ for $i,j > 1$) and therefore in this limit c^0_{eff} and d^0_{eff} are

$$c^0_{\text{eff}} = \frac{30}{1 - p^+} \rho_P \frac{cd}{c + d}, \tag{11a}$$

$$d^0_{\text{eff}} = \frac{30}{p^+} \rho_K \frac{cd}{c + d}. \tag{11b}$$

Constants c^0_{eff} and d^0_{eff} can be large in systems characterized by high densities of both kinases and phosphatases; however, according to Eqs. (11), they decrease to zero with the density of the opposing enzyme decreasing to zero.

C. Finite motility

We have analyzed two extreme cases of zero and infinite motility. In the infinite motility limit, also known as the *reaction-controlled limit*, the EMRRCs are proportional to the microscopic reaction propensities (for molecules in contact). In this limit, since $m \gg c$ and $m \gg d$, the probability that an enzyme reacts with a substrate at a single encounter is negligibly small and proportional to the microscopic rate constants c and d.

The small motility limit arises when the microscopic reaction rate constants c and d are fast when compared to motility. Processes characterized by low motility and large reaction propensities are called *diffusion limited*. For such processes the probability that an allowed reaction fires at every collision of molecules is close to 1. Therefore, for such processes EMRRCs are proportional to the collision frequency, which in turn is proportional to the motility m. Here the situation is more complex since even in the limit of zero motility the reaction rates are nonzero, as discussed in the previous section. Accordingly, one could expect the following macroscopic equation:

$$\frac{d}{dt}\rho_{S_p} = \left(\lambda m + c^0_{\text{eff}}\right) \rho_K\, \rho_{S_u} - \left(\lambda m + d^0_{\text{eff}}\right) \rho_P\, \rho_{S_p}, \tag{12}$$

where λ is some coefficient. In fact, the considered case is even more complicated, since, especially at low enzyme densities, the spatial distribution of the phosphorylated and dephosphorylated substrates is nonuniform. That is, the

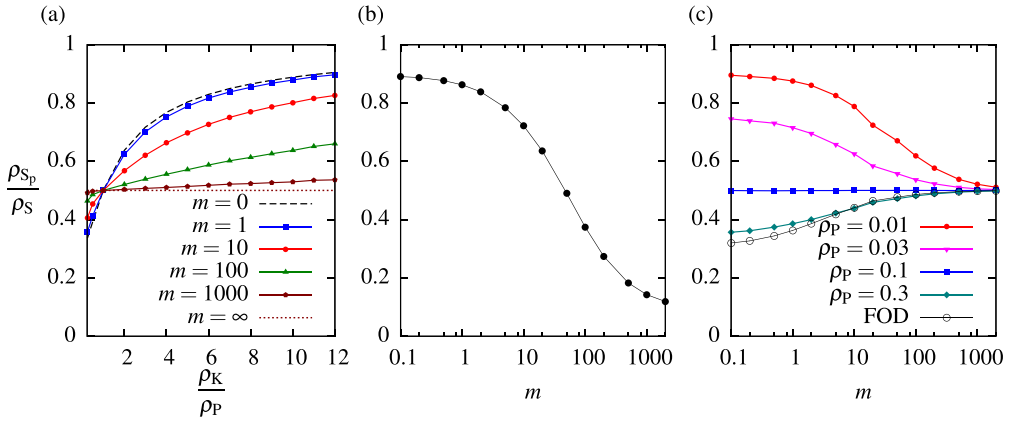

FIG. 2. (Color online) (a) Fractional density of phosphorylated substrates, ρ_{S_p}/ρ_S, as a function of the enzymes density ratio for different values of motility, m. Analytically computed limits of zero and infinite motility are marked with dashed and dotted lines. Parameters are: $\rho_S = 0.3$, $\rho_K = 0.1$, $c = 1/6\rho_K$, and $d = 1/6\rho_P$. In this series of simulations, the density of kinases was kept constant, while the density of phosphatases was varied from $\rho_P = \rho_K/0.25 = 0.4$ to $\rho_P = \rho_K/12 \approx 0.008$. By setting $d = 1/6\rho_P$, the change of phosphatases density was compensated by the proportional change of the microscopic dephosphorylation rate constant. (b) Fractional density of phosphorylated substrates as a function of m, in the case when the more abundant enzyme (kinase) has much lower catalytic activity. Simulations were performed for $\rho_S = 0.3$, $\rho_K = 0.1$, $\rho_P = 0.01$, $c = 1$, and $d = 100$. (c) Fractional density of phosphorylated substrate as a function of m for different values of phosphatase density ρ_P as well as for the first-order dephosphorylation model marked as FOD, with $d_0 = 1$. Simulations were performed for $\rho_S = 0.2$, $\rho_K = 0.1$, $c = 1/6\rho_K$, and $d = 1/6\rho_P$.

phosphorylated substrate molecules are more likely to be present in the vicinity of a kinase, while the dephosphorylated substrate molecules are more likely to be present in the vicinity of a phosphatase. As a result, even in the symmetric case of $c = d$ and $\rho_K = \rho_P$, in which the overall probability that a substrate is phosphorylated is $\frac{1}{2}$, kinase molecules collide much more often with phosphorylated substrates, which reduces the effective phosphorylation rate. Intuitively, this effect increases with decreasing density of enzymes which causes that each phosphatase molecule is surrounded by a cloud of dephospshorylated substrates and each kinase molecule by a cloud of phosphorylated substrates. We will analyze this effect in Sec. IVB by means of spatial correlation function.

As we will show below, in the general case of finite motility, EMRRCs are controlled simultaneously by the motility, both contact reaction propensities, and densities of both enzymes. Therefore, analytical determination of these rate coefficients is a challenging problem.

IV. NUMERICAL RESULTS

A. Steady-state dependence on enzyme density and motility

In this section we analyze numerically the dependence of the steady-state density of phosphorylated and dephospory-lated substrates and EMRRCs on motility and densities of the opposing enzymes. The convergence of EMRRCs to their steady state in the phosphorylation-dephosphorylation cycle is demonstrated in Appendix C. In the same appendix the nonreversible dynamics of phosphorylation in the absence of phosphatase is considered.

Let us recall that in the infinite-motility limit the effective macroscopic phosphorylation and dephosphorylation rate coefficients are $c_{\text{eff}}^{\infty} = 6c$ and $d_{\text{eff}}^{\infty} = 6d$ and, correspondingly [due to Eq. (5)], the density of phosphorylated substrates is

$$\rho_{S_p} = \frac{c\rho_K}{c\rho_K + d\rho_P}\rho_S. \tag{13}$$

To keep the steady-state densities of phosphorylated and dephosphorylated substrates equal to $\frac{1}{2}$ in the limit of the infinite motility, we keep $c\rho_K = \text{const}$ and $d\rho_P = \text{const}$, that is, we set $c = 1/6\rho_K$ and $d = 1/6\rho_P$. We found that for finite motilities the phosphorylated substrate fraction increases with ρ_K/ρ_P (in the analysis we keep $\rho_K = 0.1$ and vary ρ_P), and we show that the smaller the motility is, the more pronounced this effect is, see Fig. 2(a). The dashed line for $m = 0$ tends to 1 with ρ_K/ρ_P tending to infinity. For low motility, $m = 1$, the numerically estimated ρ_{S_p} matches closely the *zero-motility limit*. Similarly, for large motilities, ρ_{S_p} is close to the *infinite-motility limit*. Because of the symmetry, for $\rho_K = \rho_P$ the phosphorylated substrate fraction is equal to $\frac{1}{2}$ for all motilities.

In Fig. 2(b) we show that when kinases are more abundant than phosphatases, but at the same time have much lower catalytic activity, the dependence of ρ_{S_p}/ρ_S on motility is strongly pronounced. At low motilities, substrates remain mostly in the phosphorylated state, $\rho_{S_p}/\rho_S \approx 0.9$, while at high motilities they are mostly dephosphorylated, $\rho_{S_p}/\rho_S \approx 0.1$. The above shows that, generically, in the regime of low motilities (*diffusion limited*) it is the density of enzymes that decides about the state of the system and for large motilities (*reaction-controlled* limit) crucial is the product of the microscopic reaction rate constants and densities.

In Fig. 2(c) we show that the density of phosphorylated substrate can either decrease or increase with motility depending on the enzyme densities ratio. For a fixed density of kinases ($\rho_K = 0.1$) we analyze the dependence of ρ_{S_p} on motility for four values of phosphatase densities, as well as for the FOD model. Since, as in Fig. 2(a), phosphatase microscopic reaction rate constant is set $d = 1/6\rho_P$, for increasing motility, ρ_{S_p}/ρ_S tends to $\frac{1}{2}$, regardless of the phosphatase density. However, for small motilities ρ_{S_p}/ρ_S depends strongly on the phosphatase density and, in general, differs from that for the FOD model. Only for a very high density ($\rho_P = 0.3$) does

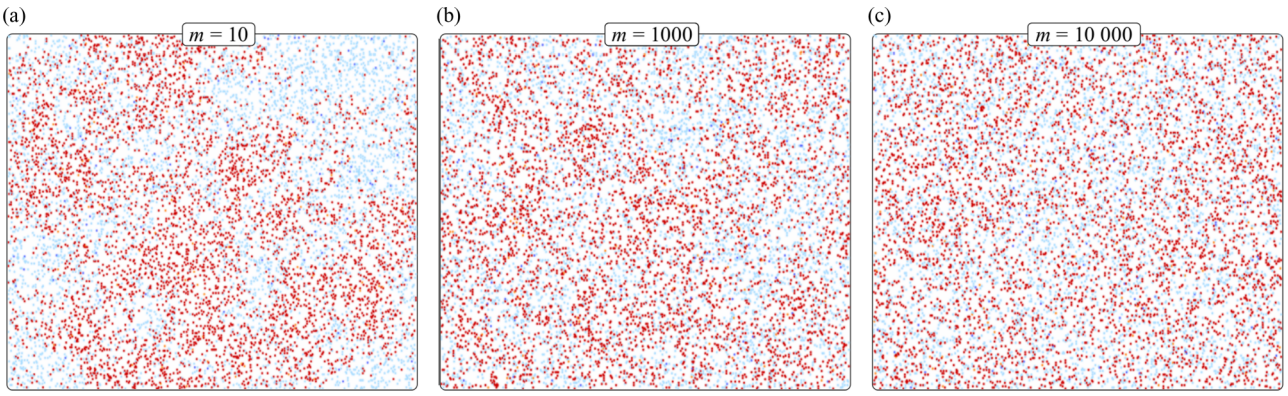

FIG. 3. (Color online) Three simulation snapshots of the 300×300 lattice showing spatial inhomogeneities of the distribution of the phosphorylated (red) and dephosphorylated (blue) substrates. For all panels $c = d = 100$, $\rho_S = 0.1$, and $\rho_K = \rho_P = 0.001$.

the fraction ρ_{S_p}/ρ_S closely match the FOD model prediction with $d_0 = 1$. This is due to the fact that for $\rho_P = 0.3$ the probability that a given substrate molecule is in contact with at least one phosphatase is high [equal to $1 - (0.7)^6 = 0.88$] and therefore the dephosphorylation is effectively of first order. This demonstrates that the FOD model cannot serve as a good approximation across a broad range of motilities.

B. Spatial correlation functions

The results shown in Fig. 2 can be explained as follows: for a decreased phosphatase density (compensated by a proportionally increased dephosphorylation rate constant d), phosphatases are surrounded by dephosphorylated substrates and therefore the effective dephosphorylation rate coefficient decreases. Intuitively, this effect becomes stronger for low motilities, for which substrates have a higher chance to be dephosphorylated after a single encounter with a phosphatase and vanishes in the limit of infinite motility, when the probability that a substrate molecule is in the phosphorylated state does not depend on its position.

It is well known that the rate of diffusion controls the steady state of the system in the case when opposing enzymes are spatially separated. As shown and discussed by Brown and Kholodenko, when substrate phosphorylation occurs at the plasma membrane and dephosphorylation occurs in the cytoplasm, gradients of phosphorylated substrates arise, and the effectiveness of the phosphorylation process depends on diffusion [48,49]. Later, van Albada and ten Wolde demonstrated that the sharpness of the response decreases with the spatial separation of opposing enzymes [50]. It was also found that although clustering reduces signal for linear reaction kinetics, it can dramatically increase signal strength in the cases when substrates require double modification [51] or there exists a positive feedback between enzymes and substrates [42,52].

Here the spatial separation of enzymes is not imposed but results from the discreteness of the matter. Park and Agmon found time-dependent concentration profiles of unconverted substrate around a solitary nonmoving enzyme molecule for the Michaelis-Menten scheme [17]. The effect of formation of inhomogeneities is visualized in Fig. 3 for three different motilities, $m \in \{10, 1000, 10\,000\}$. For small motilities clouds of phosphorylated and dephosphorylated substrates are clearly visible, whereas for larger motilities the spatial distribution of phosphorylated and dephosphorylated substrates is nearly uniform. This effect is quantified in Fig. 4 where the normalized spatial correlation functions between kinases

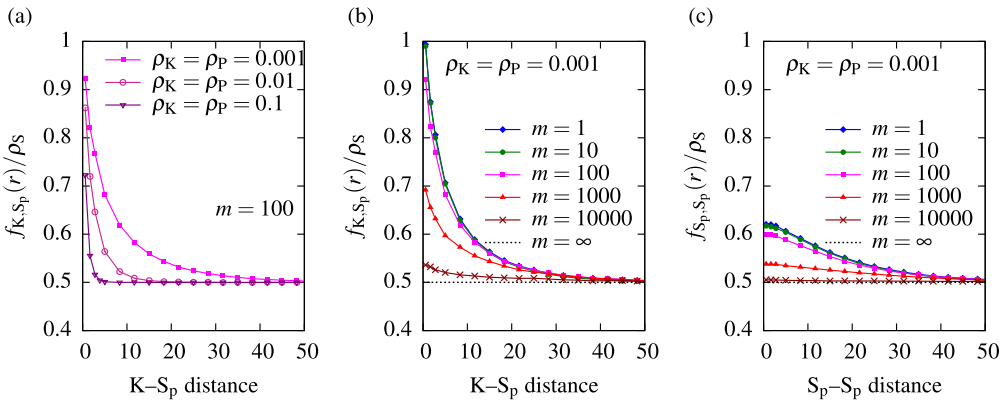

FIG. 4. (Color online) Spatial correlation functions. (a) Spatial correlation function between kinases and phosphorylated substrates $f_{K,S_p}(r)/\rho_S$ for motility $m = 100$ and three enzyme densities. (b) $f_{K,S_p}(r)/\rho_S$ for fixed enzyme densities $\rho_K = \rho_P = 0.001$ and six motilities m. (c) Spatial autocorrelation function for phosphorylated substrates $f_{S_p,S_p}(r)/\rho_S$. For all panels $c = d = 100$ and $\rho_S = 0.1$. Results shown come from averaging over 250 snapshots from independent numerical simulations on the 500×500 lattice.

and phosphorylated substrates, $f_{K,S_p}(r)/\rho_S$, and between phosphorylated substrates, $f_{S_p,S_p}(r)/\rho_S$, are plotted (r being the distance). Function $f_{K,S_p}(r)/\rho_S$ is calculated based on 250 snapshots from independent numerical simulations on the 500×500 lattice, long enough to reach the equilibrium distribution. From each snapshot, $f_{K,S_p}(r)$ is calculated as $\frac{1}{N_K}\sum_K N_{S_p}(r)/N(r)$, where N_K is the number of kinase molecules on the lattice, $N_{S_p}(r)$ is the number of phosphorylated substrates at the distance between r and $r+\Delta r$ from a given kinase, and $N(r)$ is the number of lattice sites at the distance between r and $r+\Delta r$. Then $f_{K,S_p}(r)$ is averaged over all snapshots. Function $f_{S_p,S_p}(r)/\rho_S$ is calculated analogously (i.e., the sum is over all pairs of phosphorylated substrate molecules).

As one could expect, the correlation length as well as the amplitude of the correlation function f_{K,S_p} increase with decreasing enzyme density, Fig. 4(a). Correlation length is of the order of the average distance between enzymes $1/\sqrt{\rho_K} = 1/\sqrt{\rho_P}$. For small motilities $f_{K,S_p}(1)/\rho_S \approx 1$, i.e., substrates adjacent to kinase are phosphorylated with probability close to 1. The $f_{S_p,S_p}(r)$ correlation function is smaller but the correlation length is longer. The $f_{S_p,S_p}(r)/\rho_S$ function may not reach 1 even for the smallest m, since phosphorylated substrates that are at the borders of clouds are in the close vicinity of dephosphorylated ones. The larger correlation length of $f_{S_p,S_p}(r)$ can result from fluctuations in kinase distribution. They can cause formation of transient, large "superclouds" of phosphorylated substrates surrounding several kinases. These clouds contribute to long-range correlation between phosphorylated substrates.

C. Effective macroscopic reaction rate coefficients

In this section we estimate EMRRCs on the basis of long-run numerical simulations. As was already discussed under Models and Methods, c_{eff} can be estimated according to Eq. (3). In Fig. 5 we show $c_{\text{eff}}/c^{\infty}_{\text{eff}}$ for three values of dephosphorylation rate constant d, as well as for the FOD model with $d_0 = 1$.

Effective macroscopic phosphorylation rate coefficient, c_{eff}, increases with reagents' motility and this effect is more visible for small dephosphorylation reaction rate constant d. This shows that the phosphorylation kinetics is strongly coupled with the dephosphorylation kinetics and therefore the effective macroscopic phosphorylation and dephosphorylation reaction rate coefficients cannot be estimated separately. Figure 5 shows that c_{eff} is a function of ρ_K, ρ_P, c, d, and m. The dependence of c_{eff} on motility is the strongest at the smallest considered enzyme densities, $\rho_K = \rho_P = 0.01$, see Fig. 5(c), and the weakest for the highest considered densities, $\rho_K = \rho_P = 0.2$, see Fig. 5(a), where $c^0_{\text{eff}}/c^{\infty}_{\text{eff}}$ is large. This, consistently with Fig. 2, is due to the fact that at high enzyme densities, substrates are constantly in contact with both kinases and phosphatases, and thus the phosphorylation and dephosphorylation reactions can occur almost independently of the diffusion. As shown for $\rho_K = \rho_P = 0.2$ and $\rho_K = \rho_P = 0.05$, Figs. 5(a) and 5(b), numerically estimated c_{eff} for $m = 0.1$ matches well the analytically calculated limit of c^0_{eff}; for $\rho_K = \rho_P = 0.01$, Fig. 5(c), the agreement is worse since the convergence of $c_{\text{eff}}(m)$ to c^0_{eff} is slower.

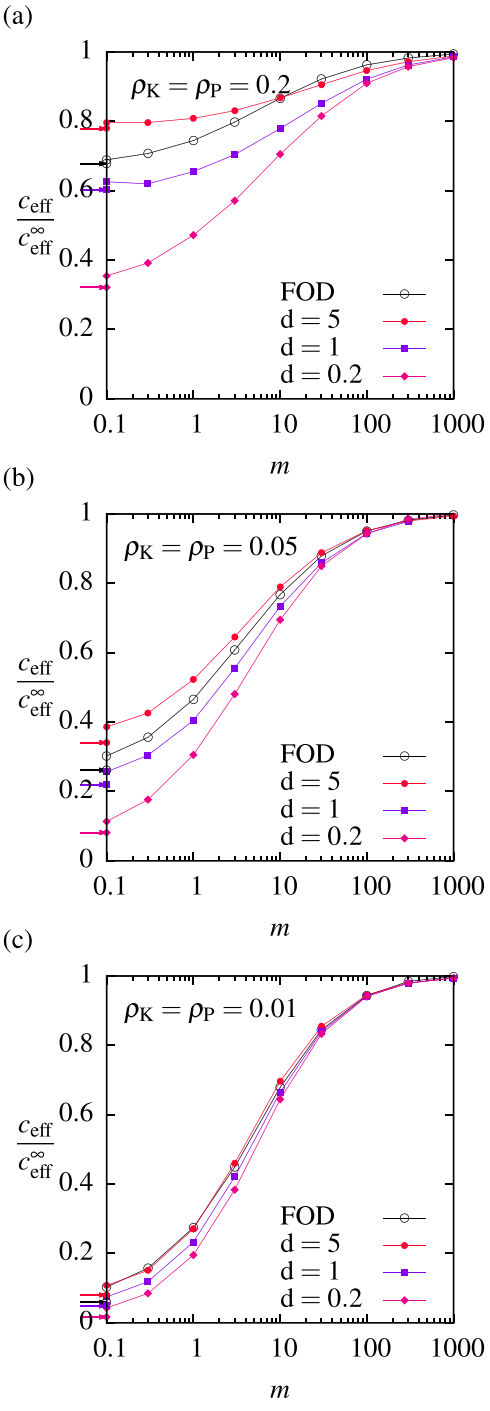

FIG. 5. (Color online) Scaled effective macroscopic phosphorylation rate coefficient $c_{\text{eff}}/c^{\infty}_{\text{eff}}$ as a function of motility m. Densities of enzymes are $\rho_K = \rho_P = 0.2$ in (a), $\rho_K = \rho_P = 0.05$ in (b), and $\rho_K = \rho_P = 0.01$ in (c). First-order dephosphorylation model marked as FOD, with $d_0 = 6\rho_P$, which corresponds to $d = 1$ in the basic model. Analytically calculated c^0_{eff} are marked by respective arrows next to the vertical axis. For all panels $\rho_S = 0.3$, $c = 1$.

We will now analyze these effects in the limit when phosphorylation is a diffusion-driven process. As discussed above, such a limit can be achieved when diffusion-independent reactions are very infrequent compared to those driven by

diffusion, i.e., when

$$c_{\text{eff}}^0 \ll \lambda m, \quad d_{\text{eff}}^0 \ll \lambda m. \tag{14}$$

Simultaneously, the microscopic reaction rate constants, c and d, should be much larger than motility, so the probability of a reaction firing at a collision is close to 1,

$$c \gg m, \quad d \gg m. \tag{15}$$

These conditions are difficult to satisfy in numerical simulations, therefore to estimate the diffusion-limited contribution, λm, we subtract the analytically calculated zero-motility rate constant c_{eff}^0 from the numerically estimated c_{eff}. We will here assume high reaction propensities, $c = d = 1000$, and consider motilities $m \in [0,1000]$ and enzyme densities $\rho_E \in [0.0001, 0.1]$. The EMRRC is estimated, as previously, from long-run numerical simulations on the 100×100 lattice, based on Eq. (3).

First we investigate the symmetric case of $\rho_K = \rho_P =: \rho_E$. In Fig. 6(a) we show the dependence of $c_{\text{eff}}/c_{\text{eff}}^\infty$ on enzyme densities in a log-log scale for seven values of motility. The numerical predictions for small motilities, $m = 1$ and $m = 3$, lie close the theoretical prediction of the *zero-motility limit* (dashed line). It shows that for relatively small motilities and large enzyme densities the zero-motility contribution is a substantial part of the overall effective rate. The theoretically predicted c_{eff}^0 is the lower bound for the effective rate coefficient. The zero-motility contribution is proportional to the enzyme density and thus for intermediate motilities, $m \in \{10,30\}$, it becomes dominant as enzyme density increases.

In order to eliminate the zero-motility contribution from the effective rate coefficient, we show $(c_{\text{eff}} - c_{\text{eff}}^0)/c_{\text{eff}}^\infty$ with respect to enzyme densities [Fig. 6(b)] and with respect to motility [Fig. 6(c)]. In light of Eq. (12) we would expect $c_{\text{eff}} - c_{\text{eff}}^0 = \lambda m$ and therefore $(c_{\text{eff}} - c_{\text{eff}}^0)/c_{\text{eff}}^\infty$ to be proportional to m for fixed densities of enzymes, which is confirmed in Fig. 6(c). The average of gradients of lines on the log-log plot is equal to 0.99. We therefore numerically confirmed our heuristic prediction that in the small motility limit:

$$c_{\text{eff}} = c_{\text{eff}}^0 + \lambda(\rho_E) m. \tag{16}$$

Figure 6(b) confirms that the coefficient λ decreases (weakly) with decreasing enzyme density. As discussed in Sec. IVB, this dependence follows from the fact that, at low enzyme densities, enzymes are surrounded by clouds of converted substrates. This effect is quantified in Fig. 4(a) showing that spatial correlation function between kinase and phosphorylated substrate increases (in both amplitude and correlation length) with decreasing density of enzymes. The effective reaction rate is proportional to the density of unconverted substrates in lattice sites adjacent to the enzyme site. Therefore, it decreases to zero when the correlation function tends to 1 in $r = 1$ (adjacent sites).

D. Molecular crowding: Steady-state dependence on crowders' motility

Here we investigate the molecular crowding effect, i.e., we analyze how the densities of active substrates in the stationary state change due to the presence of additional molecules,

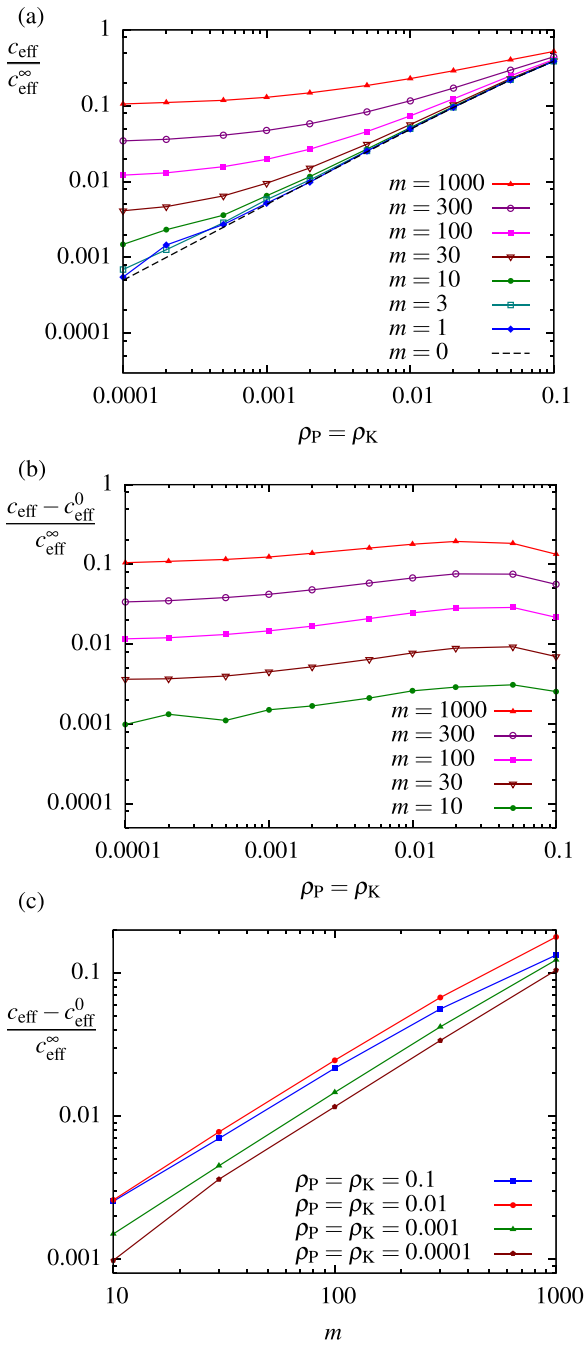

FIG. 6. (Color online) (a) Scaled effective macroscopic phosphorylation rate coefficient $c_{\text{eff}}/c_{\text{eff}}^\infty$ as a function of enzyme density $\rho_K = \rho_P$. (b) Scaled effective macroscopic phosphorylation rate constant with subtracted zero-motility contribution: $(c_{\text{eff}} - c_{\text{eff}}^0)/c_{\text{eff}}^\infty$ with respect to enzyme density. (c) $(c_{\text{eff}} - c_{\text{eff}}^0)/c_{\text{eff}}^\infty$ with respect to motility. For all panels $c = d = 1000$.

crowding agents, which do not react but occupy space and diffuse with a given motility m_C, not necessarily equal to m.

As shown in Fig. 9 in Appendix B, the presence of crowding agents leads to the decrease of effective motility of reacting molecules and this decrease is more pronounced for small motilities of crowding molecules and large motilities of reacting molecules [Fig. 9(b) versus Fig. 9(a)]. The reduction of the effective substrate motility either increases the fraction

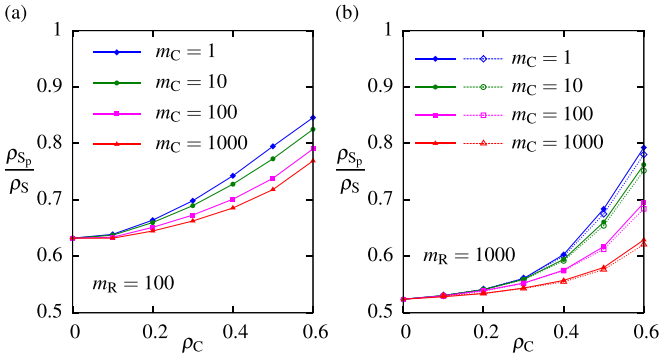

FIG. 7. (Color online) Phosphorylated substrate fractional density with respect to the density of crowding agents ρ_C. Reagents motility $m_R = 100$ in (a), $m_R = 1000$ in (b), and for four values of crowding agents motility m_C. Dashed lines refer to the simulations without crowding agents, with scaled reagents motility $\tilde{m}$, see Eq. (17). Other parameters are $\rho_S = 0.2$, $\rho_K = 0.09$, $\rho_P = 0.01$, $c = 1/6\rho_K$, and $d = 1/6\rho_P$.

of phosphorylated substrates in the stationary state, provided that $\rho_K > \rho_P$, or, because of the symmetry of the model, decreases this fraction for $\rho_P > \rho_K$. As shown in Fig. 7(b), the effect of crowding agents can be almost fully reproduced by the appropriate scaling of reagents motility,

$$\tilde{m}_R := m_R \frac{m_{\text{eff}}(\rho_R,\rho_C,m_R,m_C)}{m_{\text{eff}}(\rho_R,m_R)}, \tag{17}$$

where $\rho_R = \rho_S - \rho_K - \rho_P$ is the fractional density of all reacting molecules assumed to have the same motility m_R. In the numerator of Eq. (17) there is the effective motility of reacting molecules of density ρ_R and motility m_R in the presence of crowding agents of density ρ_C and motility m_C, estimated in numerical simulations and given in Fig. 9(b). In the denominator of Eq. (17) there is the effective motility of reacting molecules of density ρ_R and motility m_R in the absence of additional molecules, given by the approximate Eq. (B5). This shows that the presence of chemically inert molecules can substantially change the balance between opposing reactions.

V. DISCUSSION

We investigated the correspondence between microscopic and macroscopic reaction rate coefficients in the model of the phosphorylation-dephosphorylation cycle with respect to diffusion (motility). The biological membrane is simplified to a two-dimensional triangular lattice where molecules are allowed to move with given motilities and react when in adjacent lattice sites with given propensities: microscopic reaction rate constants. Based on numerical simulations we estimated the steady state of the system (fraction of phosphorylated substrates) as well as EMRRCs as functions of reaction propensities, fractional densities of substrates, and motility. There are two opposing limits of infinite and zero motility, for which the EMRRC steady states were calculated analytically and confirmed numerically.

In the infinite motility limit, the positions of molecules are independent and therefore the macroscopic reaction rate is proportional to the product of enzyme and substrate densities and reaction propensities. This implies that the macroscopic reaction rate coefficients are equal to the microscopic propensities multiplied by the number of potential neighbors (which is 6 in our case of the triangular lattice). In this limit of infinite motility, the probability that a reaction fires at a substrate-enzyme collision is (infinitely) small and proportional to reaction propensity, and therefore the process can be considered as *reaction limited*.

In the limit of zero motility, reactions can occur only for the substrates which remain in contact with the opposing enzymes and therefore the zero-motility reaction rate coefficients decrease to zero with enzyme densities decreasing to zero, but can be significant for dense systems. In realistic conditions the limit of zero motility can be approached in very dense systems in which the effective diffusion is very low due to molecular crowding, and the probability that a substrate is trapped in contact with the opposing enzymes is high. This limit gives the lower bound for the effective reaction rate coefficients for nonzero motility.

For finite (small, but nonzero) motility we have shown the emergence of the contribution (proportional to molecules' motility) stemming from *diffusion-limited* reactions. In this regime (almost) all enzyme-substrate collisions lead to reactions. The most challenging is the regime of intermediate motilities, in which we found (based on numerical simulations) that the EMRRCs (and steady states of the system) depend in a nontrivial way on all microscopic reaction propensities and fractional densities of substrates. Precisely, the effective phosphorylation rate coefficient depends not only on the microscopic phosphorylation rate constant and kinase density but also on the dephosphorylation rate constant and phosphatase density. The parameters describing the activity and density of opposing enzymes influence the spatial distribution of phosphorylated substrate and, consequently, the probability that, e.g., a kinase molecule will collide with a dephosphorylated substrate. Generally, small enzyme densities give rise to clouds of phosphorylated and dephosphorylated substrates surrounding respective enzymes. However, the analytical estimation of macroscopic parameters for intermediate motility requires, and in our opinion deserves, more effort.

The analysis of the influence of molecular crowding on the steady state of the system showed that the presence of crowding molecules can be accounted for by modifying effective motility of reagents. Quite surprisingly, a system without crowding molecules but with appropriately reduced reagents motility predicts almost the same steady state as the system with crowding molecules. We have quantified the influence of molecular crowding on the effective motility of reagents and provided a semianalytical formula for the mentioned scaling.

The phosphorylation-dephosphorylation cycle was analyzed under the simplifying assumption in which the phosphorylation and dephosphorylation are treated as single-step reactions. In reality these processes involve at least three steps and require formation of a transient enzyme-substrate complex. In Appendix D we consider a model in which an enzyme and substrate can form a transient complex; we show that while enzyme-substrate binding is relatively short and, correspondingly, the enzyme sequestration is low, this more detailed model predicts almost the same steady states as the

original, more coarse-grained, model. In the case of more stable enzyme-substrate binding, we found that the level of enzyme (and substrate) sequestration substantially increases with motility and that, consequently, the sequestration modifies (quantitatively) steady-state dependence on motility. Analysis of this case requires further study.

In summary, our analysis is a step towards the determination of effective macroscopic reaction rate coefficients and steady states for ubiquitous cycles of opposing reactions with respect to the motility of substrates and enzymes and their densities. The presence of two antagonistic enzymes and discreteness of reacting substances lead to inhomogeneities in the phosphorylated and dephosphorylated substrate distribution. These inhomogeneities are large for slow diffusion and small enzyme densities, as indicated by spatial correlation functions. As a result, the effective catalytic activities depend on the diffusivity and enzymes densities: In the example presented in Fig. 2(b) kinases "win" at low motility, while at high motility phosphatases dominate, rendering most of the substrate dephosphorylated.

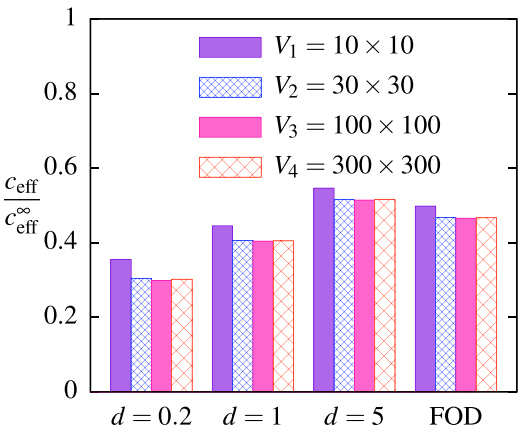

FIG. 8. (Color online) Scaled effective macroscopic phosphorylation rate coefficient $c_{\rm eff}/c^{\infty}_{\rm eff}$, estimated in simulations performed on lattices of different sizes. For all simulations $\rho_S = 0.3$, $c = 1$, $m = 1$, and $\rho_K = \rho_P = 0.05$. In the first-order dephosphorylation, model marked as FOD, $d_0 = 6\rho_P$, which corresponds to $d = 1$ in the basic model. The difference between the 10×10 lattice and the remaining lattices is statistically significant, the differences between larger lattices are of order of the statistical error.

ACKNOWLEDGMENTS

The research for this paper was in part supported by the EU through the European Social Fund, Contract No. UDA-POKL.04.01.01-00-072/09-00. P.S. and M.K. were supported by Polish National Science Center Grant No. NCN-KR-0011/253/2/13. J.M. thanks the Polish National Science Center for support under Grant No. 2011/01/B/NZ2/00864. T.L. was supported by Polish National Science Center Grant No. 2011/03/B/NZ2/00281. Numerical simulations were carried out using the Zeus computer cluster in Krakow and the Grafen supercomputer of the Ochota Biocenter.

APPENDIX A: DEPENDENCE OF EMRRCS ON THE LATTICE SIZE

Here we analyze the influence of the lattice size on the estimated EMRRCs (see Fig. 8). The simulations were performed on lattices 300×300, 100×100, 30×30, and 10×10. For each lattice size and each parameter set [corresponding to parameters chosen for Fig. 5(b)] we performed 10 independent simulations with simulation times $t = 10^3$, $t = 9 \times 10^3$, $t = 100 \times 10^3$, $t = 900 \times 10^3$, i.e., inversely proportional to the lattice size, which assured that more than 5×10^4 reactions fired in each simulation. Each simulation was preceded by an equilibration phase lasting for 1000. We calculated the scaled effective macroscopic phosphorylation rate coefficient $c_{\rm eff}/c^{\infty}_{\rm eff}$ independently for each simulation, and then, based on the set of 10 simulations (for each lattice size and each parameter set), we calculated the mean value of $c_{\rm eff}/c^{\infty}_{\rm eff}$ and the error of the mean. In each case the error of the mean was found smaller than 10^{-3}. In conclusion, we found that for assumed densities of molecules the differences between the 10×10 lattice and the remaining lattices are significant, while the differences between larger latices are of the order of the statistical error. One could expect that the dependence of EMRRCs on the lattice size can be stronger for systems of smaller molecule densities. In the analyzed system there are 45 phosphatases, 45 kinases, and 300 substrates on the 30×30 lattice.

APPENDIX B: MACROSCOPIC DIFFUSION COEFFICIENT AS A FUNCTION OF MOTILITY AND MOLECULES DENSITY

Here, in order to study the impact of molecular crowding on the phosphorylation-dephosphorylation kinetics, we analyze the impact of crowding agents on effective diffusion coefficient. The macroscopic diffusion coefficient, D, of a single tracer molecule having motility m depends on the total density of the crowding molecules ρ_C (i.e., the fraction of lattice sites occupied by molecules), their motility $m_C = m/\gamma$, and the lattice constant ℓ:

$$D = f(\rho_C,\gamma)(1-\rho_C)\ell^2 m/4, \tag{B1}$$

where f is the correlation function that can be approximated by the following formula [53,54]:

$$f(\rho_C,\gamma) = \frac{\left\{[(1-\gamma)(1-\rho_C)f_0 + \rho_C]^2 + 4\gamma(1-\rho_C)f_0^2\right\}^{1/2} - [(1-\gamma)(1-\rho_C)f_0 + \rho_C]}{2\gamma(1-\rho_C)f_0}, \tag{B2}$$

where

$$f_0 = (1-\alpha)/[1+\alpha(2\gamma-1)]. \tag{B3}$$

The coefficient α depends on the lattice type; for the triangular lattice (considered here) $\alpha = 0.282$, for the square lattice $\alpha = 1 - 2/\pi$, and for the honeycomb (or hexagonal) lattice

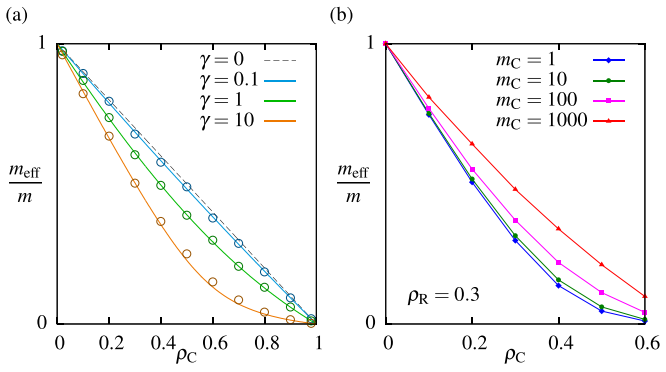

FIG. 9. (Color online) Scaled effective motility $m_{\rm eff}/m$ as a function of density of crowding molecules ρ_C and motility $m_C = m/\gamma$. (a) Effective motility of a tracer molecule in the presence of crowding molecules. Lines correspond to the theoretical result given by Eq. (B1), and circles mark results of corresponding numerical simulations. (b) Scaled effective motility $m_{\rm eff}/m$ of reacting molecules with fractional density $\rho_R = 0.3$ and motility $m = 1000$ in the presence of crowders. This result is used in simulations shown in Fig. 7(b).

$\alpha = 1/2$ [55]. The parameter $m_{\rm eff} = f(\rho_C,\gamma)(1-\rho_C)m$ will be considered as the effective motility of the tracer molecule in the presence of crowding molecules of density ρ_C and motility m_C.

The correlation function f satisfies $0 < f < 1$ for $0 < \gamma < \infty$. In the limit of $\gamma \to 0$, i.e., when crowding molecules move infinitely fast and a tracer molecule does not sense their positions, $f \to 1$; in the limit of $\gamma = \infty$, i.e., when crowding molecules do not move, the expression for f reads:

$$f(\rho_C) = \max\left\{0, \frac{(1-\alpha)-\rho_C(1+\alpha)}{(1-\rho_C)(1-\alpha)}\right\}. \tag{B4}$$

According to the equation above, the diffusion coefficient of a tracer molecule drops to zero when the fractional density of immobile obstacles equals $\rho_{\rm crit} = (1-\alpha)/(1+\alpha) = 0.56$, which agrees reasonably well with the percolation threshold of 1/2 for the triangular lattice. In the case most interesting to us, i.e., when all molecules have the same motility ($\gamma = 1$), Eq. (B1) simplifies to

$$D(\rho_C,1) = \frac{\sqrt{\rho_C^2 + 4(1-\rho_C)\left(\frac{1-\alpha}{1+\alpha}\right)^2} - \rho_C}{2\left(\frac{1-\alpha}{1+\alpha}\right)}\ell^2 m/4. \tag{B5}$$

The approximate Eq. (B1) agrees well with our simulation results presented in Fig. 9(a). In these simulations we estimated the effective motility of the tracer molecule $m_{\rm eff} := \langle {\rm Dist}^2\rangle/\Delta t$, based on the mean-square distance $\langle {\rm Dist}^2\rangle$ covered by the tracer molecule in time Δt. To obtain reasonable statistics at a modest computational cost we performed simulations in which the number of tracer molecules was larger than 1 but always smaller than 1% of the number of crowding molecules. Finally, in order to analyze the influence of crowding molecules with a given motility on the effective motility of reacting molecules, we performed simulations in which the density of reacting molecules was 30%, while different densities and motilities of crowding molecules were considered, see Fig. 9(b). These results are used in Sec. IV D to interpret the effect of molecular crowding on the steady state of the reacting system.

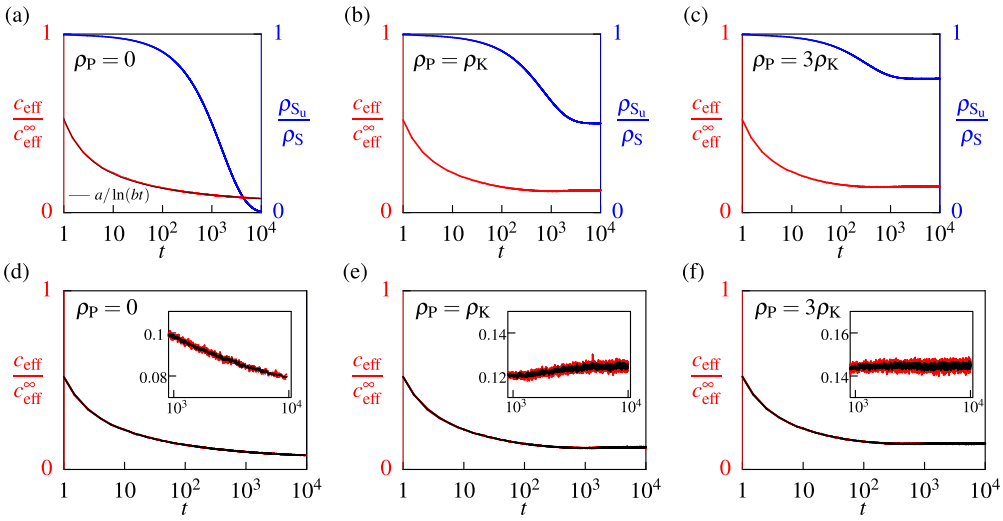

FIG. 10. (Color online) Scaled effective macroscopic phosphorylation rate coefficient $c_{\rm eff}/c_{\rm eff}^\infty$ and fractional density of phosphorylated substrates ρ_{S_p}/ρ_S as a function of time with initial density of phosphorylated substrate set zero. Simulations were performed for $\rho_K = 0.001$, $\rho_S = 0.3$, $m = 1$, $c = 1$, and $d = 1$. Two cases are considered: nonreversible phosphorylation (a) with $\rho_P = 0$ and a reversible phosphorylation-dephosphorylation cycle (b) and (c) with $\rho_P = \rho_K$ and $\rho_P = 3\rho_K$. The curves in panels (a), (b), and (c) result from averaging over 1000 independent simulations performed on the 300×300 lattice. In the nonreversible case, the fraction of dephosphorylated substrate drops to 0.5% at the end of simulations, leading to substantial fluctuations in the effective macroscopic phosphorylation rate coefficient. Coefficients of the fitting function in (a) are $a = 5.044$ and $b = 1.586$. In panels (d), (e), and (f) we compare $c_{\rm eff}(t)/c_{\rm eff}^\infty$ estimates based on 1000 simulations (black line) with the estimates based on 333 simulations (three red lines). The trajectories for $t > 1000$ are shown in the insets.

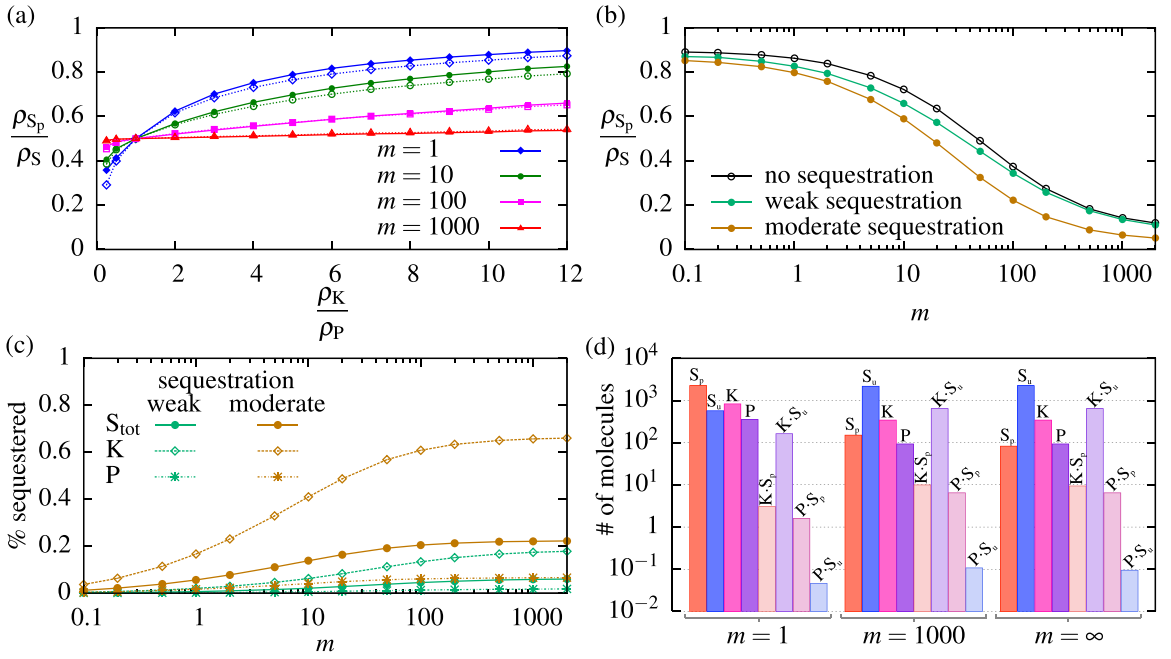

FIG. 11. (Color online) (a) Fractional density of phosphorylated substrates as a function of the enzyme ratio for different values of motility m. We compare the model variant in which the formation of a transient enzyme-substrate complex is explicitly included [the case of weak enzyme sequestration, Eqs. (D2); dotted lines] with the original model prediction shown in Fig. 2(a) (solid lines). The parameters used in the simulations of the basic (original) model: $\rho_S = 0.3$, $\rho_K = 0.1$, $c = 1/6\rho_K$, $d = 1/6\rho_P$; the parameters for the model variant considered are defined by Eqs. (D2). In the calculation of the phosphorylated substrate fraction only free (unbound) substrates are considered. (b) Fractional density of phosphorylated substrates as a function of m. We compare the original model prediction shown in Fig. 2(b) (black line) with the model variant in which the formation of a transient enzyme-substrate complex is explicitly included; two cases are considered: weak sequestration, Eqs. (D2), and moderate enzyme sequestration, Eqs. (D3). The parameters used in simulations are $\rho_S = 0.3$, $\rho_K = 0.1$, $\rho_P = 0.01$, $c = 1$, and $d = 100$. (c) Fraction of sequestered reactants for the weak and moderate sequestration cases as a function of m in simulations performed for (b). (d) Steady-state densities of all reactants and complexes in the case of moderate sequestration, Eqs. (D3), for three motilities: $m = 1$, $m = 1000$, and $m = \infty$. Values for finite motility come from simulations performed for (b). Values for infinite motility are given by the steady state of the corresponding system of ODEs.

APPENDIX C: SYSTEM EQUILIBRATION

In this appendix we numerically analyze system relaxation to the steady state. Within the framework of our main model we consider irreversible and reversible dynamics with the initial condition in which all substrates are dephosphorylated. In the irreversible case, Fig. 10(a), we assume that phosphatases are absent, while in the reversible case we assume that the density of phosphatases is either equal to, or 3 times higher than, the density of kinases, Figs. 10(b) and 10(c). In both cases, since at $t = 0$ all substrates are dephosphorylated, there is no correlation between the position of a substrate molecule and its phosphorylation status. Therefore, in the limit of $t \to 0$, the scaled effective macroscopic phosphorylation rate coefficient $c_{\text{eff}}/c_{\text{eff}}^{\infty} \to 1$; however, on the time scale of $1/c$ (when substrates being in contact with kinases are phosphorylated) it decreases to lower values.

In the irreversible case, Fig. 10(a), $\rho_{S_p}/\rho_S \to 0$, while the effective macroscopic phosphorylation rate coefficient decreases slowly with time. Torney and McConnel [11] showed theoretically that in two dimensions (in contrast to three dimensions) the reaction rate coefficient of the irreversible reaction $A + B \to \emptyset$ decreases logarithmically in time. The fit shown in Fig. 10(a) suggests that also for our reaction, $K + S_u \to K + S_p$, the reaction rate coefficient decreases logarithmically as $a/\ln(bt)$, where $a = 5.044$ and $b = 1.586$.

In the reversible case considered in this study [see Figs. 10(b) and 10(c)], we observe that the effective macroscopic phosphorylation rate coefficient, as well as the density of phosphorylated substrate ρ_{S_p}/ρ_S, converge to the (positive) steady-state values. Interestingly, the convergence of the effective macroscopic phosphorylation rate coefficient is about one order of magnitude faster than the convergence of ρ_{S_p}/ρ_S, which shows that the steady-state values of EMRRCs can serve as a good approximation also when the system is far from its steady state.

The effective macroscopic phosphorylation rate coefficient shown in Figs. 10(a), 10(b), and 10(c) was calculated based on Eq. (3a) by averaging over 1000 independent simulations on the 300×300 lattice. The time interval Δt was adjusted in such a way that the cumulative number of reactions (in 1000 simulations) is not smaller than 50 000. Therefore, in the reversible case, Δt is of order 1 during the whole simulation, while in the irreversible case (in which the frequency of phosphorylation events decreases substantially) Δt increases from 1 to about 200 at the end of simulation time. Since the time derivative of $c_{\text{eff}}(t)/c_{\text{eff}}^{\infty}$ also decreases, the increase of Δt does not contribute substantially to the error.

To demonstrate the accuracy of our $c_{\mathrm{eff}}(t)/c_{\mathrm{eff}}^{\infty}$ numerical estimates, in Figs. 10(d), 10(e), and 10(f), we compared the estimates based on 1000 simulations with three estimates, each based on 333 simulations. The difference between estimates based on 1000 and 333 simulations is visible only in the close-ups (insets).

APPENDIX D: ANALYSIS OF THE MODEL WITH TRANSIENT ENZYME–SUBSTRATE COMPLEXES

The phosphorylation-dephosphorylation cycle was analyzed under the simplifying assumption in which the phosphorylation and dephosphorylation are treated as single-step reactions. In reality, these processes involve at least three steps and require formation of a transient enzyme-substrate complex. It is therefore important to verify whether the analyzed effects are preserved when the more accurate description is considered. In the more detailed model, reactions (1) are replaced by

$$K + S_u \underset{c_2}{\overset{c_1}{\rightleftharpoons}} \{K \cdot S_u\} \xrightarrow{c_3} \{K \cdot S_p\} \xrightarrow{c_4} K + S_p, \quad \text{(D1a)}$$

$$P + S_p \underset{d_2}{\overset{d_1}{\rightleftharpoons}} \{P \cdot S_p\} \xrightarrow{d_3} \{P \cdot S_u\} \xrightarrow{d_4} P + S_u, \quad \text{(D1b)}$$

where curly brackets denote substrate complex.

We consider two sets of reaction rate constants corresponding to the short or longer enzyme-substrate binding, implying, respectively, either weak or stronger but still moderate enzyme sequestration. The constants for the two cases are

weak sequestration:

$$c_1 = 2c, \quad c_2 = 10c, \quad c_3 = 10c, \quad c_4 = 100c, \quad \text{(D2a)}$$

$$d_1 = 2d, \quad d_2 = 10d, \quad d_3 = 10d, \quad d_4 = 100d; \quad \text{(D2b)}$$

moderate sequestration:

$$c_1 = 10c, \quad c_2 = 9c, \quad c_3 = c, \quad c_4 = 100c, \quad \text{(D3a)}$$

$$d_1 = 10d, \quad d_2 = 9d, \quad d_3 = d, \quad d_4 = 100d. \quad \text{(D3b)}$$

For these two sets of constants a substrate being initially in contact with an enzyme molecule is modified with almost the same probability as in the original model. For this model variant we performed an analysis analogous to that shown in Fig. 2 (see Fig. 11). In the case of weak sequestration, we obtained the quantitatively similar dependence of fraction of phosphorylated substrate on enzyme density and on motility [Figs. 11(a) and 11(b)] as in the original model.

For stronger sequestration, for which the fraction of sequestered kinase exceeds 60% (for large motilities), the agreement with the original model [Fig. 11(b)] is only qualitative. Importantly, the fraction of sequestered enzymes and substrates significantly grows with motility. This is due to the fact that the increase of motility implies more enzyme-substrate encounters, and therefore increases their binding rate, not influencing the dissociation rate.

Overall, the analysis of the above model variant shows that the reported dependence of steady state on motility is independent of the details of the phosphorylation and dephosphorylation processes, as long as the fractions of sequestered enzymes and substrate are small, and results from the presence of opposing enzymes in the reaction network. However, for stronger enzyme-substrate binding, the fraction of sequestered reactants is higher (and dependent on their motility), and therefore the quantitative dependence of the phosphorylated substrate fraction on motility can differ and requires further study.

[1] F. C. Collins and G. E. Kimball, J. Colloid Sci. **4**, 425 (1949).
[2] R. J. Ellis, Curr. Opin. Struct. Biol. **11**, 114 (2001).
[3] D. Hall and A. P. Minton, Biochim. Biophys. Acta **1649**, 127 (2003).
[4] J. S. Kim and A. Yethiraj, Biophys. J. **96**, 1333 (2009).
[5] E. C. Stites, P. C. Trampont, Z. Ma, and K. S. Ravichandran, Science **318**, 463 (2007).
[6] M. von Smoluchowski, Z. Phys. Chem. **92**, 129 (1917).
[7] D. Fange, O. G. Berg, P. Sjöberg, and J. Elf, Proc. Natl. Acad. Sci. U.S.A. **107**, 19820 (2010).
[8] S. Hellander, A. Hellander, and L. Petzold, Phys. Rev. E **85**, 042901 (2012).
[9] K. R. Naqvi, Chem. Phys. Lett. **28**, 280 (1974).
[10] C. A. Emeis and P. L. Fehder, J. Am. Chem. Soc. **92**, 2246 (1970).
[11] D. C. Torney and H. M. McConnell, Proc. R. Soc. London A **387**, 147 (1983).
[12] D. Toussaint and F. Wilczek, J. Chem. Phys. **78**, 2642 (1983).
[13] C. E. Allen and E. G. Seebauer, J. Chem. Phys. **104**, 2557 (1996).
[14] A. Szabo, J. Phys. Chem **93**, 6929 (1989).
[15] H. Kim, M. Yang, M.-U. Choi, and K. J. Shin, J. Chem. Phys. **115**, 1455 (2001).
[16] S. Park and N. Agmon, J. Phys. Chem. B **112**, 5977 (2008).
[17] S. Park and N. Agmon, J. Phys. Chem. B **112**, 12104 (2008).
[18] H.-X. Zhou, J. Phys. Chem. B **101**, 6642 (1997).
[19] Y. B. Zel'dovich and A. A. Ovchinnikov, JETP Lett **26**, 440 (1977).
[20] O. G. Berg, J. Chem. Phys. **31**, 47 (1978).
[21] N. Agmon and A. Szabo, J. Chem. Phys. **92**, 5270 (1990).
[22] A. Szabo, J. Chem. Phys. **95**, 2481 (1991).
[23] J. Sung and S. Lee, J. Chem. Phys. **111**, 796 (1999).
[24] A. L. Edelstein and N. Agmon, J. Phys. Chem. **99**, 5389 (1995).
[25] K. Takahashi, S. Tanase-Nicola, and P. Rein ten Wolde, Proc. Natl. Acad. Sci. U.S.A. **107**, 2473 (2010).
[26] J. S. van Zon, M. J. Morelli, S. Tanase-Nicola, and P. R. ten Wolde, Biophys. J. **91**, 4350 (2006).
[27] C. C. Govern, M. K. Paczosa, C. A. K, and E. S. Huseby, Proc. Natl. Acad. Sci. U.S.A. **107**, 8724 (2010).
[28] A. V. Popov and N. Agmon, J. Chem. Phys. **117**, 5770 (2002).
[29] S. Park, K. J. Shin, and N. Agmon, J. Chem. Phys. **121**, 868 (2004).
[30] S. Park, K. J. Shin, A. V. Popov, and N. Agmon, J. Chem. Phys. **123**, 034507 (2005).
[31] A. Szabo and H.-X. Zhou, B. Kor. Chem. Soc. **33**, 925 (2012).

[32] A. P. Minton, J. Biol. Chem. **276**, 10577 (2001).
[33] S. Schnell and T. E. Turner, Prog. Biophys. Mol. Biol. **85**, 235 (2004).
[34] Z. Kalay, T. K. Fujiwara, and A. Kusumi, PLoS ONE **7**, e32948 (2012).
[35] K. Aoki, K. Takahashi, K. Kaizu, and M. Michiyuki, Sci. Rep. **3** (2013).
[36] M. Weiss, Phys. Rev. E **88**, 010101 (2013).
[37] M. Kochańczyk, J. Jaruszewicz, and T. Lipniacki, J. R. Soc. Interface **10**, 20130151 (2013).
[38] P. J. Zuk, M. Kochańczyk, J. Jaruszewicz, W. Bednorz, and T. Lipniacki, Phys. Biol. **9**, 055002 (2012).
[39] D. T. Gillespie, J. Phys. Chem **81**, 2340 (1977).
[40] A. B. Bortz, M. H. Kalos, and J. L. Lebowitz, J. Comput. Phys. **17**, 10 (1975).
[41] Y. Kuramoto, Prog. Theor. Phys. **52**, 711 (1974).
[42] B. Hat, B. Kazmierczak, and T. Lipniacki, PLoS Comput. Biol. **7**, e1002197 (2011).
[43] P. Tolar, H. W. Sohn, W. Liu, and S. K. Pierce, Immunol. Rev. **232**, 34 (2009).
[44] R. J. Brezski and J. G. Monroe, in *Multichain Immune Recognition Receptor Signaling* (Springer, Berlin, 2008), pp. 12–21.
[45] N. E. Harwood and F. D. Batista, Annu. Rev. Immunol. **28**, 185 (2009).
[46] H. Husebye, Ø. Halaas, H. Stenmark, G. Tunheim, Ø. Sandanger, B. Bogen, A. Brech, E. Latz, and T. Espevik, EMBO J. **25**, 683 (2006).
[47] J. Pękalski, A. Ciach, and N. G. Almarza, J. Chem. Phys. **140**, 114701 (2014).
[48] G. C. Brown and B. N. Kholodenko, FEBS Lett. **457**, 452 (1999).
[49] B. N. Kholodenko, Nat. Rev. Mol. Cell Biol. **7**, 165 (2006).
[50] S. B. van Albada and P. R. ten Wolde, PLoS Comput. Biol. **3**, e195 (2007).
[51] A. Mugler, A. Bailey, K. Takahashi, and P. R. ten Wolde, Biophys. J. **102**, 1069 (2012).
[52] B. Kazmierczak and T. Lipniacki, J. Theor. Biol. **259**, 291 (2009).
[53] H. van Beijeren and R. Kutner, Phys. Rev. Lett. **55**, 238 (1985).
[54] P. Almeida and W. Vaz, Handb. Biol. Phys. **1**, 305 (1995).
[55] K. Compaan and Y. Haven, Trans. Farad. Soc. **52**, 786 (1956).